Bayesian Machine Learning in metamaterial design
Fragile becomes supercompressible

Bessa, Miguel A.; Głowacki, Piotr; Houlder, Michael

Important note
To cite this publication, please use the final published version (if applicable).
Please check the document version above.

Bayesian Machine Learning in Metamaterial Design: Fragile Becomes Supercompressible

Miguel A. Bessa,* Piotr Glowacki, and Michael Houlder

Designing future-proof materials goes beyond a quest for the best. The next generation of materials needs to be adaptive, multipurpose, and tunable. This is not possible by following the traditional experimentally guided trial-and-error process, as this limits the search for untapped regions of the solution space. Here, a computational data-driven approach is followed for exploring a new metamaterial concept and adapting it to different target properties, choice of base materials, length scales, and manufacturing processes. Guided by Bayesian machine learning, two designs are fabricated at different length scales that transform brittle polymers into lightweight, recoverable, and supercompressible metamaterials. The macroscale design is tuned for maximum compressibility, achieving strains beyond 94% and recoverable strengths around 0.1 kPa, while the microscale design reaches recoverable strengths beyond 100 kPa and strains around 80%. The data-driven code is available to facilitate future design and analysis of metamaterials and structures (https://github.com/mabessa/F3DAS).

Structure-dominated materials (metamaterials) are pushing the envelope of known electromagnetic,[1] classic,[2] and quantum[3] mechanical properties by exploring new geometries. Additive manufacturing has been a major driving force in this exploration since virtually any topology can be obtained to probe the vast design space created by geometric changes in the material structure. This has led to discoveries of materials with new properties and functionality, for example exhibiting negative linear compressibility,[4] tunable negative stiffness,[5] controllable reconfigurability via programmable surfaces[6] or via origami,[7] and symmetry breaking elastic surface patterns.[8] However, metamaterial design has relied on extensive experimentation and a trial-and-error approach where analytical or computational models only provide a posteriori explanations. Here, we argue in favor of inverting the process by using a computational

data-driven approach to explore new design possibilities, while reducing experimentation to a minimum (validation).

Without loss of generality, we illustrate this paradigm shift by focusing on a new concept for a low density mechanical metamaterial (**Figure 1**). The aim is to additively manufacture a building block that achieves recoverable supercompressibility while maintaining high strength and stiffness. This concept results from a combination of a deployable mast[9,10] developed for highly deformable space structures, and a thin-walled conical frustum[11] common in impact absorption applications.

Remarkably, even without inverting the design process, additively manufactured mechanical metamaterials with low densities ($\rho \ll 1$ g cm^{-3}) have achieved compressive strengths above 100 MPa while exhibiting brittle fracture using carbon lattices,[12] on the order of 1 MPa with partially recoverable compressive strains in excess of 50% using microlattices of alumina[13] or graphene aerogels,[14] and on the order of 0.5 kPa and exceeding 80% strains for another graphene aerogel.[15] These investigations demonstrate that tuning the geometry of the metamaterial to explore symmetry-breaking instabilities (buckling) is the key to achieve large effective compressibility while causing small deformation of a high strength base material. Yet, the process for designing these metamaterials and assessing their mechanical limits is cumbersome and time-consuming due to the absence of general design principles arising from highly nonlinear, unstable, and imperfection sensitive responses that depend on many geometric parameters. More importantly, even when successful designs are found,[12–15] tuning them for new applications requiring different properties and functionality is not trivial. In this context, machine learning can provide significant advantages to the design process.

Machine learning and deep learning are already able to surpass the limits of a human mind in specific tasks. Algorithms are capable of winning against human champions in increasingly difficult games,[16–18] they recognize faces with near human-level accuracy,[19] and predict ratings of unseen movies based on past user selection.[20] These achievements are permeating to different scientific disciplines such as materials science[21,22] and chemistry,[23] and recently they are reaching the design of electromagnetic metamaterials via nonprobabilistic machine[24] and deep learning[25–28] methods, and even generative deep learning.[29] However, metamaterials usually derive their unprecedented properties from exploring imperfection-sensitive behavior because

Prof. M. A. Bessa, P. Glowacki, M. Houlder
Department of Materials Science and Engineering
Delft University of Technology
2628 CD Delft, The Netherlands
E-mail: M.A.Bessa@tudelft.nl

The ORCID identification number(s) for the author(s) of this article can be found under https://doi.org/10.1002/adma.201904845.

ADVANCED
SCIENCE NEWS
www.advancedsciencenews.com

ADVANCED
MATERIALS
www.advmat.de

Longeron

D_2

P

D_1

Support ring

Arbitrary
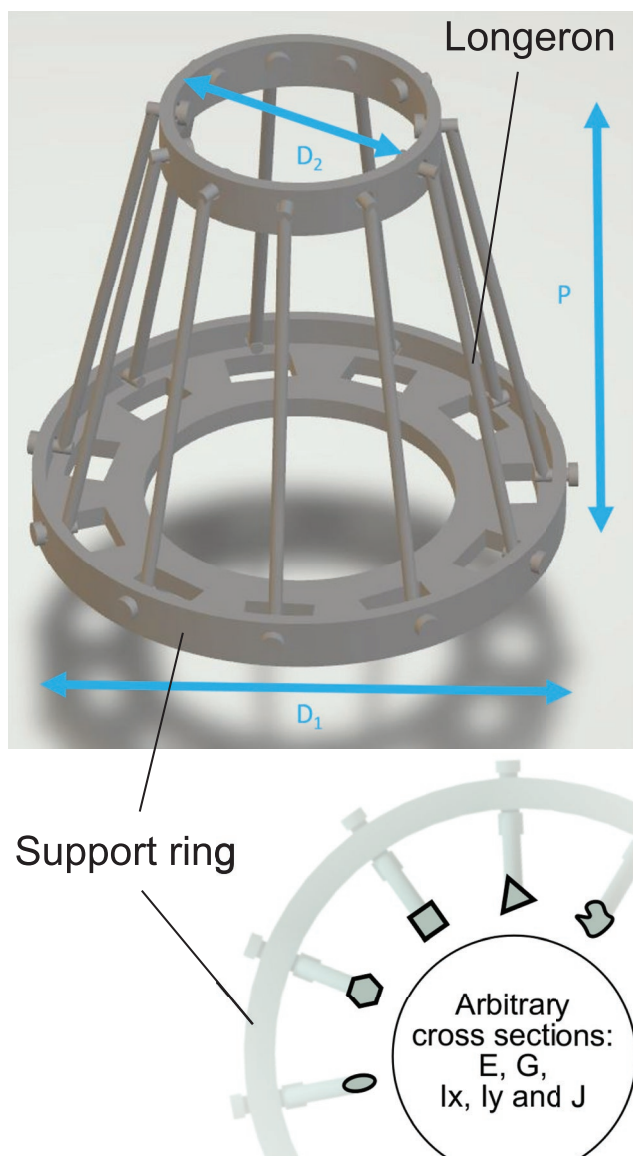cross sections:
E, G,
Ix, Iy and J

Figure 1. Supercompressible metamaterial building block with generalized cross-section for the longerons (x is the radial direction; y is the tangential direction).

they operate at extreme regimes. In these cases, Bayesian methods become important because they deal with noisy observations by inferring a smooth average response and quantifying uncertainty. The key novelty of our work is the consideration of these methods to design and analyze a new mechanical metamaterial.

Broadly, there are two classes of Bayesian methods that can be useful to analyze and design metamaterials: 1) Bayesian machine learning;[30] 2) Bayesian optimization.[31] Here, we focus on Bayesian machine learning because our goal is to create a map of the solution space that can be used later for robust optimization of different applications. However, if the goal was to find only one optimum metamaterial for a specific application, then Bayesian optimization methods are likely to be more effective because they seek the optimum solution by adaptively sampling the solution space in a trade-off between

exploration and exploitation. The Supporting Information includes two sections ("Why Bayesian machine learning?" and "Bayesian machine learning vs Bayesian optimization") with additional references and considerations for the interested reader.

Our data-driven exploration follows a recent framework created to design materials and structures.[32,33] This modular framework integrates: 1) design of experiments to sample the input variables, 2) efficient predictive analyses to generate the output database, 3) machine learning to establish input–output relationships from the database, and 4) optimization to determine optimum designs from the machine learning model. Different methods can be chosen for each module depending on the problem's dimensionality, size of database needed for the learning process, and whether the phenomena of interest is probabilistic or deterministic. Our mechanical metamaterial undergoes probabilistic responses due to buckling/postbuckling mechanisms, and involves a moderate number of design parameters that is expected to lead to large training datasets. Recent Bayesian machine learning methods called sparse Gaussian processes[30] have been developed to fulfill these requirements while being sufficiently scalable. We considered several algorithms, as detailed in the Supporting Information ("Sparse Gaussian processes: scalability & accuracy"), and concluded that the sparse Gaussian process regression (SGPR) algorithm[34] was the most adequate for the regression tasks, while the scalable variational Gaussian process classification (SVGP)[35] was the most adequate for classification.

Data-driven design of the metamaterial concept is then summarized in **Figure 2**. First, the building block (Figure 1) is parameterized according to the design variables. The geometry is defined by the top and bottom base diameters, D_1 and D_2, height P, and four parameters that define the cross-section of the vertical elements (longerons): the cross-sectional area A, moments of inertia I_x and I_y, and torsional constant J_τ. In addition, since the metamaterial is targeted to be reversibly deformable, any chosen base material is defined by its elastic constants: the Young's modulus E and the shear modulus G. Given that this is a nonlinear elastic mechanics problem, we know a priori that the geometric variables can be scaled by one of the dimensions, chosen here as D_1, and that we can consider the ratio of elastic constants G/E. Finally, since no contact between the deformed longerons is intended, their number is not a variable due to the principle of superposition, i.e., increasing the number of longerons leads to a proportional increase of the compressive strength. All seven input variables and respective bounds of the design space are defined in Table S1, Supporting Information.

Different designs are then generated by sampling this bounded space according to a Sobol sequence[36] (Figure 2A), since this design of experiments method facilitates the subsequent learning process.[32] The response of each design is then predicted via nonlinear finite element analyses (Figure 2B) that provide the complete buckling and postbuckling behavior (Figure 2C) by the arc-length method.[33] Each simulation of the virtual design predicts the effective compressive strains and stresses of the metamaterial, from which two quantities of interest can be computed: critical buckling stress σ_{crit} and elastic energy absorption E_{abs}. The critical buckling stress σ_{crit} represents the point at which the instability starts, from which the structure no longer behaves as linearly elastic. The elastic
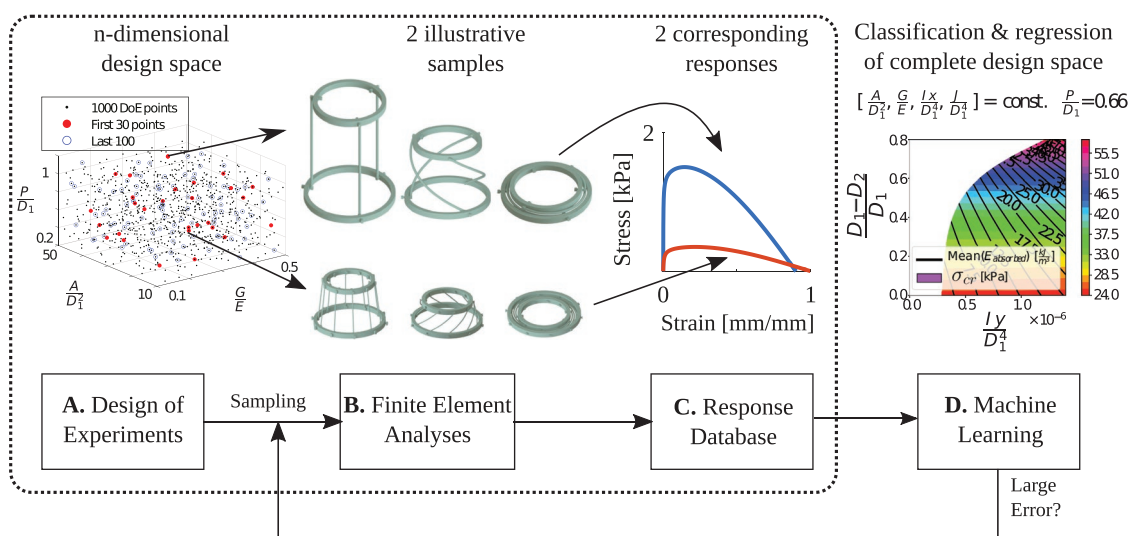
1904845 (2 of 6)

Figure 2. Data-driven design of supercompressible metamaterial building block using seven design variables.

energy absorption E_{abs} is defined as the area below the complete stress–strain response. These quantities of interest are stored in a large database (over 100 000 simulations) that can then be analyzed by machine learning (Figure 2D).

For this problem, both machine learning classification and regression are useful. Classification allows to distinguish between relevant and irrelevant regions of the design space, as many combinations of parameters lead to metamaterials that do not coil when subjected to compression (invalidating supercompressibility). For example, global deformation modes in bending or local buckling phenomena of the longerons. Based on the buckling modes predicted by eigenvalue finite element analyses, we can classify the designs as: 1) coilable or 2) noncoilable. Figure 2D shows a projection of the design space obtained by the machine learning model, where the white region in the contour plot corresponds to noncoilable designs. Then, we can limit the regression task to the coilable regions and predict how the quantities of interest are changing (see colored region of Figure 2D). The color gradient in the figure represents changes of the average critical buckling stress (in kPa), and the labeled black isolines show how the average energy absorption of the different designs evolves in the same projection of the design space (in kJ m^{-3}). We refer to Figures S7–S9, Supporting Information where different projections of the design space are shown, and to Figure S10, Supporting Information for different stress–strain responses of three different designs, including uncertainty.

Machine learning's practical relevance is first illustrated by targeting a recoverable and highly compressible design manufactured by fused filament fabrication using polylactic acid (PLA) (**Figure 3**). This inexpensive manufacturing process creates parts with defects, so it is challenging to create slender elements. Therefore, simplifying the cross-section of the longerons is advantageous. Figure 3A shows the results of a global Sobol sensitivity analysis[37] obtained by probing the seven input parameter machine learning model of Figure 2D. Since the first sensitivity indices of every variable contribute almost entirely to the respective total sensitivity, there is minimal high-order

input interaction, i.e., if the values are close to 1, then that input strongly influences the output, and if close to zero, its influence is negligible. Figure 3A demonstrates that the cross-sectional area A of the longerons is irrelevant for both quantities of interest, and that the ratio of elastic moduli G/E has negligible influence when compared with the moments of inertia of the longerons. Also, independently of the cross-section shape, the moments of inertia are complementary because I_x affects more the critical buckling stress, while I_y affects more the absorbed energy. Interestingly, the torsional constant J_τ has a strong influence on the critical buckling stress, but not on the absorbed energy (detailed analyses in the Supporting Information).

We can then restrict to manufacturing designs with circular cross-sections for the longerons, reducing I_x, I_y, and J_τ to a single independent variable: the cross-section diameter d. Since A and G/E are negligible, the remaining variables that compose the design space are the height P and relative base diameters $(D_1 - D_2)/D_1$. This reduces the design space to only three dimensions, which are easy to visualize (Figure 3B). In addition, when considering printable designs made of brittle base materials (PLA), the local strains at the longerons need to be predicted throughout the complete deformation process in order to know if the metamaterial is undergoing plasticity or fracture. We conducted elementary experimental tests to characterize the base material which supported the use of a simplified yield criterion: maximum local strain needs to be below 2%. Classifying the design space according to this criterion shows many geometric solutions that, despite being coilable (blue region in Figure 3B), create high local deformations causing plasticity or fracture before the metamaterial is fully compressed. The inset in Figure 3B represents the corresponding variation of the quantities of interest in the reversibly coilable region (yellow region).

Based on the classification and regression results, we manufactured and tested six different designs to validate the classification boundaries. Figure 3C,D shows the design with highest compressibility, where the final length reduces to the thickness of the bottom ring, leading to a total compressive
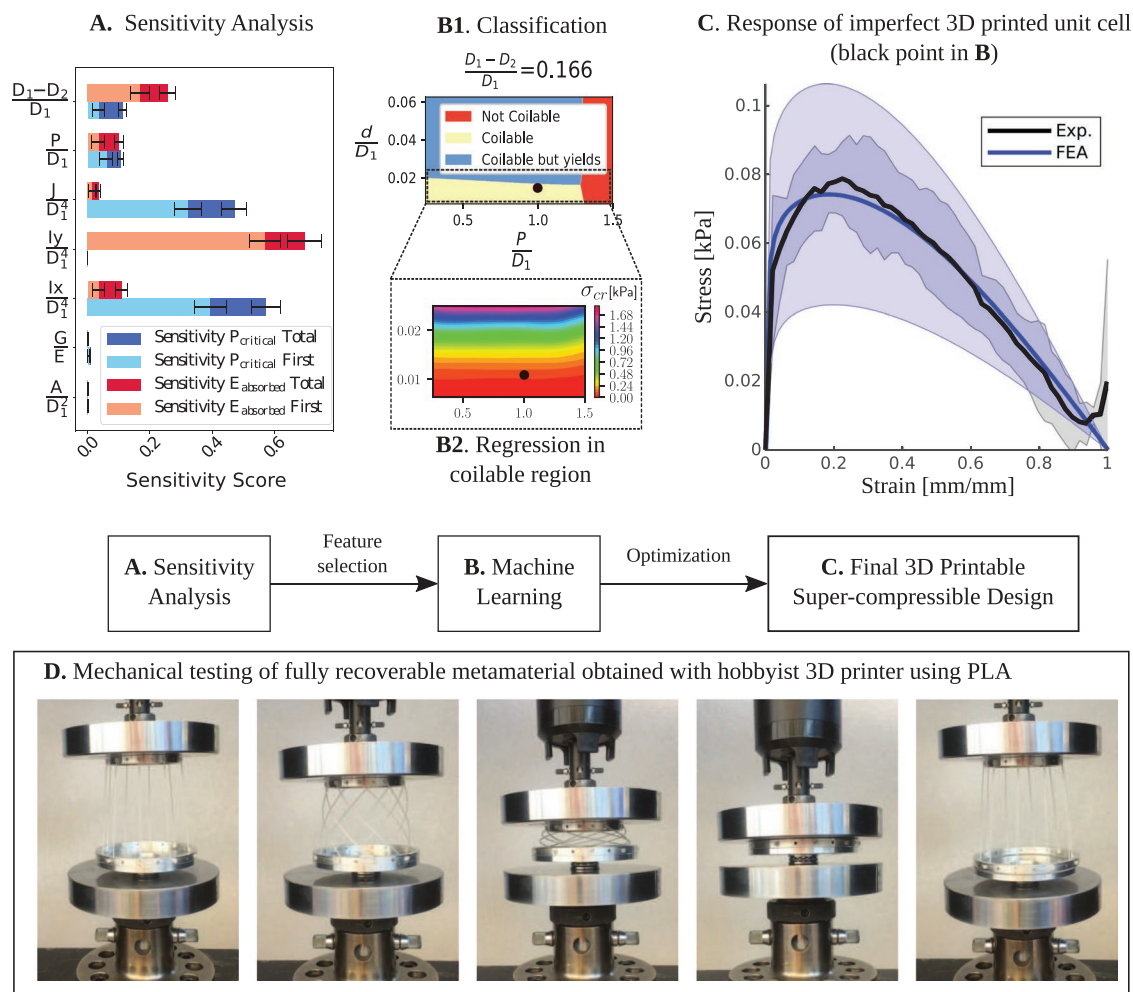
Figure 3. Design of fully recoverable metamaterial with nearly 100% compressibility printable with hobbyist 3D printer using PLA. Design leads to local maximum strains below 2%. The experiments were conducted for D_1 = 90 mm, D_2 = 75 mm, P = 60 mm, d = 1 mm, and 10 longerons. In (C), the effective compressive strain shown does not consider the thickness of the support rings (measured maximum effective strain was 94% due to using rings with nonoptimized thickness; note that the maximum value achievable would be 98.3%, where the final configuration height would be the longerons' diameter (see Figure S16, Supporting Information for clarity)). In addition, the shaded regions in (C) correspond to the 95% confidence intervals of the experiments and simulations, respectively. The source of uncertainty in the simulations can be seen in Table S3 and Figure S4, Supporting Information.

strain of 95% and complete recoverability. This is unlike current additively manufactured solutions reviewed above. Figure 3C includes a comparison between experiments and finite element predictions taking into account the propagation of uncertainty from the input properties to the response of the metamaterial. The Supporting Information provides additional details about input uncertainty, simulations, and experiments in other regions of the design space.

Note, however, that the data-driven approach to design relies on the accuracy of the computational predictions (database). The next illustrative example shows that computer models often miss important information when confronted with reality, but even in this case, machine learning can be useful. When attempting to downscale the design by nanofabricating the unit cell, we faced an additional complication not taken into account by our finite element predictions: the photoresist resin we used for nanofabrication contracts significantly after curing,

leading to an undesired distortion of the metamaterial even before applying a load. We circumvented this challenge by conducting the data-driven design on a monolithic concept, i.e., we maintained the unit cell but connected the longerons through horizontal elements (**Figure** 4A). Once again machine learning showed that monolithic designs were possible (Figure S16, Supporting Information), although postcure contraction is not included in the predictions. Nevertheless, the design charts allowed us to navigate the space in an informed manner, minimizing our iterations to three until we reached a viable unit cell where the longeron diameter was sufficiently large to withstand the distorting effects of postcure contraction, while still being close to a region of full recoverability.

We conducted two different experiments for testing the microscale monolithic metamaterial. In the experiment summarized in Figure 4, we considered successively longer deformation cycles until we reached maximum
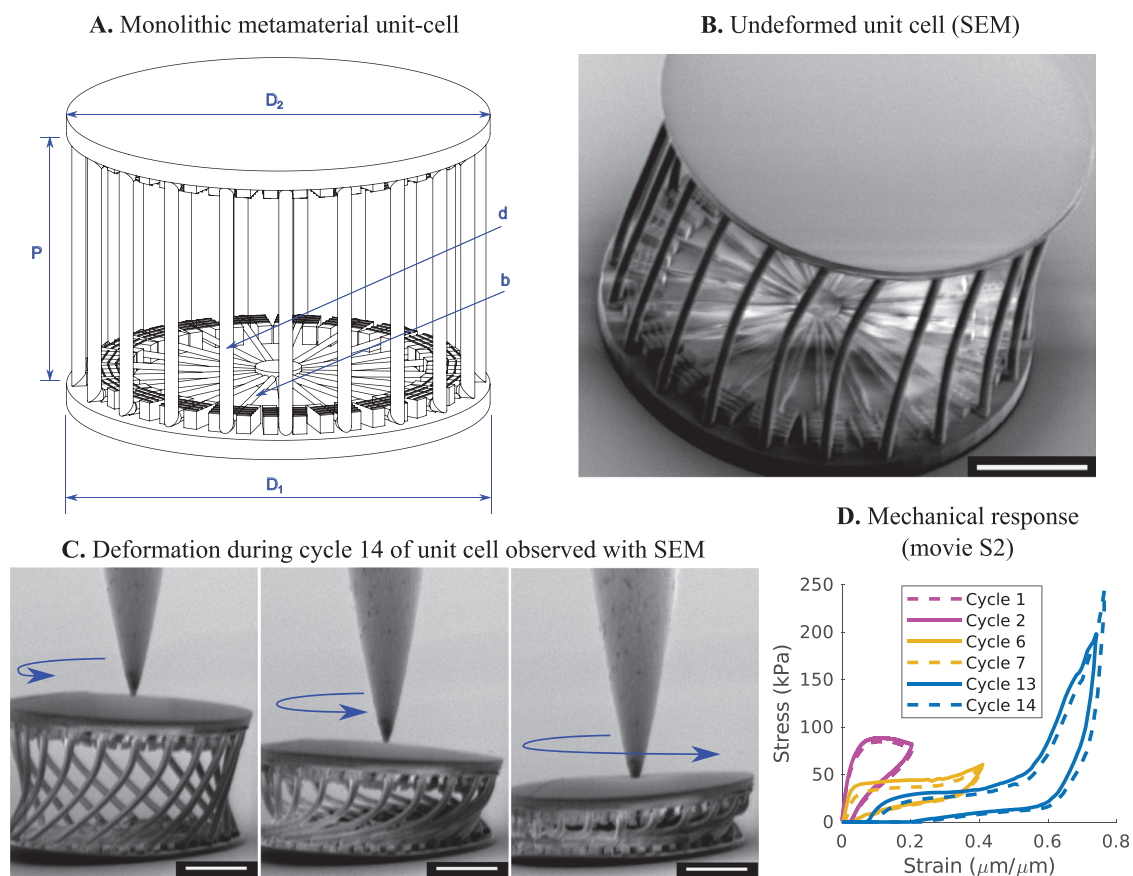
**ADVANCED
SCIENCE NEWS**

www.advancedsciencenews.com

**ADVANCED
MATERIALS**

www.advmat.de

A. Monolithic metamaterial unit-cell

B. Undeformed unit cell (SEM)

C. Deformation during cycle 14 of unit cell observed with SEM

D. Mechanical response
(movie S2)

Figure 4. Monolithic metamaterial obtained with two-photon nanolithography with geometry defined by bottom and top support ring diameters, respectively, $D_1 = D_2 = 200$ µm, height $P = 120$ µm, 21 longerons with diameter $d = 7$ µm, and horizontal battens with diameter $b = 3.5$ µm. The white bars correspond to 50 µm. (D) shows only a few loading cycles for clarity, but the complete experiment is shown in Figure S21, Supporting information. We recommend watching Movie S2, Supporting Information of the metamaterial undergoing cycle 14 (after being compressed in stages for 13 times). In addition, Figure S20, Supporting Information refers to a different experiment where the metamaterial is fully compressed at every cycle and observed with an optical microscope (see also Movie S1, Supporting Information).

compressibility. This experiment demonstrates the recoverability of every cycle, since each cycle is repeated at least once. Figure S20, Supporting Information shows more data about this experiment, including more cycles than showed in Figure 4D and additional images of the metamaterial (see also Movie S2, Supporting Information). Furthermore, the Supporting Information also includes a second experiment where we tested maximum compressibility for every loading–unloading cycle (see Figure S19 and Movie S1, Supporting Information).

In conclusion, we demonstrate that inverting the design process from experimentally guided to data-driven is possible and advantageous even when computational models are missing some information. This approach is widely applicable to design and analyze different materials and structures. For example, stretch-dominated and bending-dominated lattice structures[38–40] can be designed and optimized under uncertainty in a similar way. The essential requisites are that "enough" data about the problem of interest is available, and that the data is sufficiently accurate. This data does not need to be exclusively computational, as it could also be analytical or experimental. Therefore, we believe that machine learning will play an

ever-increasing role in the quest for the best materials, but it is in tuning them for unforeseen scenarios where it may be most attractive to use it.

Experimental Section

Fabrication and Testing of Macroscale Specimens: Based on the classified regions shown in Figure 3B, the metamaterial was manufactured with top and bottom support rings in aluminum, while 3D printing the longerons in PLA via fused filament fabrication (Ultimaker 2+). The aluminum rings minimized friction at the hinges because the finite element analyses did not include the effect of friction. Specimens were also manufactured completely in PLA and the designs were viable, but the compressive strength increased due to friction (in this case, the finite element analyses underpredicted strength). Specimens were tested in a standard mechanical testing device.

Fabrication and Testing of Microscale Specimens: The microscale monolithic specimens were manufactured by two-photon nanolithography using the Photonic Professional GT system (Nanoscribe GmbH, Germany) with a high resolution objective (63×) and IP-Dip photoresist. Samples were developed in a propylene glycol methyl ether acetate (PGMEA) bath for 30 min followed by a second bath in isopropyl alcohol (IPA) for about 2 min. SolidWorks was used for the computer-aided design and Describe for compiling the data into the

system. A nanomechanical testing device (FemtoTools, Switzerland) was used for the compression tests observed by an optical microscope or a scanning electron microscope (SEM).

Supporting Information

Supporting Information is available from the Wiley Online Library or from the author.

Acknowledgements

Conflict of Interest

The authors declare no conflict of interest.

Keywords

[1] N. I. Zheludev, Y. S. Kivshar, *Nat. Mater.* **2012**, *11*, 917.
[2] K. Bertoldi, V. Vitelli, J. Christensen, M. van Hecke, *Nat. Rev. Mater.* **2017**, *2*, 17066.
[3] A. L. Rakhmanov, A. M. Zagoskin, S. Savel'ev, F. Nori, *Phys. Rev. B* **2008**, *77*, 144507.
[4] A. B. Cairns, J. Catafesta, C. Levelut, J. Rouquette, A. van der Lee, L. Peters, A. L. Thompson, V. Dmitriev, J. Haines, A. L. Goodwin, *Nat. Mater.* **2013**, *12*, 212.
[5] M. Serra-Garcia, J. Lydon, C. Daraio, *Phys. Rev. E* **2016**, *93*, 010901.
[6] C. Coulais, E. Teomy, K. de Reus, Y. Shokef, M. van Hecke, *Nature* **2016**, *535*, 529.
[7] J. T. B. Overvelde, J. C. Weaver, C. Hoberman, K. Bertoldi, *Nature* **2017**, *541*, 347.
[8] N. Stoop, R. Lagrange, D. Terwagne, P. M. Reis, J. Dunkel, *Nat. Mater.* **2015**, *14*, 337.
[9] S. Pellegrino, *Deployable Structures*, Springer, Vienna **2001**, pp. 1–35
[10] L. Puig, A. Barton, N. Rando, *Acta Astronaut.* **2010**, *67*, 12.
[11] N. Gupta, N. M. Sheriff, R. Velmurugan, *Thin-Walled Struct.* **2006**, *44*, 986.
[12] J. Bauer, A. Schroer, R. Schwaiger, O. Kraft, *Nat. Mater.* **2016**, *15*, 438.
[13] L. R. Meza, S. Das, J. R. Greer, *Science* **2014**, *345*, 1322.
[14] C. Zhu, T. Y.-J. Han, E. B. Duoss, A. M. Golobic, J. D. Kuntz, C. M. Spadaccini, M. A. Worsley, *Nat. Commun.* **2015**, *6*, 6962.
[15] L. Qiu, B. Huang, Z. He, Y. Wang, Z. Tian, J. Z. Liu, K. Wang, J. Song, T. R. Gengenbach, D. Li, *Adv. Mater.* **2017**, *29*, 1701553.
[16] M. Campbell, A. Hoane, F.-h. Hsu, *Artif. Intell.* **2002**, *134*, 57.
[17] A. Lally, J. M. Prager, M. C. McCord, B. K. Boguraev, S. Patwardhan, J. Fan, P. Fodor, J. Chu-Carroll, *IBM J. Res. Dev.* **2012**, *56*, 2:1.
[18] D. Silver, A. Huang, C. J. Maddison, A. Guez, L. Sifre, G. van den Driessche, J. Schrittwieser, I. Antonoglou, V. Panneershelvam, M. Lanctot, S. Dieleman, D. Grewe, J. Nham, N. Kalchbrenner, I. Sutskever, T. Lillicrap, M. Leach, K. Kavukcuoglu, T. Graepel, D. Hassabis, *Nature* **2016**, *529*, 484.
[19] Y. Taigman, M. Yang, M. Ranzato, L. Wolf, in *Proc. of the IEEE Conf. on Computer Vision and Pattern Recognition (CVPR)*, IEEE, Piscataway, NJ, USA **2014**, pp. 1701–1708.
[20] R. Bell, Y. Koren, C. Volinsky, *Computer* **2009**, *42*, 30.
[21] S. Curtarolo, D. Morgan, K. Persson, J. Rodgers, G. Ceder, *Phys. Rev. Lett.* **2003**, *91*, 135503.
[22] R. Gautier, X. Zhang, L. Hu, L. Yu, Y. Lin, T. O. Sunde, D. Chon, K. R. Poeppelmeier, A. Zunger, *Nat. Chem.* **2015**, *7*, 308.
[23] D. T. Ahneman, J. G. Estrada, S. Lin, S. D. Dreher, A. G. Doyle, *Science* **2018**, *360*, 186.
[24] Q. Zhang, C. Liu, X. Wan, L. Zhang, S. Liu, Y. Yang, T. J. Cui, *Adv. Theory Simul.* **2019**, *2*, 1800132.
[25] I. Malkiel, M. Mrejen, A. Nagler, U. Arieli, L. Wolf, H. Suchowski, *Light: Sci. Appl.* **2018**, *7*, 60.
[26] W. Ma, F. Cheng, Y. Liu, *ACS Nano* **2018**, *12*, 6326.
[27] T. Qiu, X. Shi, J. Wang, Y. Li, S. Qu, Q. Cheng, T. Cui, S. Sui, *Adv. Sci.* **2019**, *6*, 1900128.
[28] Z. Liu, D. Zhu, S. P. Rodrigues, K.-T. Lee, W. Cai, *Nano Lett.* **2018**, *18*, 6570.
[29] W. Ma, F. Cheng, Y. Xu, Q. Wen, Y. Liu, *Adv. Mater.* **2019**, *31*, 1901111.
[30] Z. Ghahramani, *Nature* **2015**, *521*, 452.
[31] J. González, Z. Dai, P. Hennig, N. Lawrence, in *Proc. of the 19th Int. Conf. on Artificial Intelligence and Statistics* (Eds: A. Gretton, C. C. Robert), Microtome Publishing, Brookline, MA, USA **2016**, pp. 648–657.
[32] M. Bessa, R. Bostanabad, Z. Liu, A. Hu, D. W. Apley, C. Brinson, W. Chen, W. Liu, *Comput. Methods Appl. Mech. Eng.* **2017**, *320*, 633.
[33] M. Bessa, S. Pellegrino, *Int. J. Solids Struct.* **2018**, *139–140*, 174.
[34] J. Hensman, A. G. Matthews, M. Filippone, Z. Ghahramani, in *Advances in Neural Information Processing Systems 28* (Eds: C. Cortes, N. D. Lawrence, D. D. Lee, M. Sugiyama, R. Garnett), Curran Associates, Inc., Red Hook, NY, USA **2015**, pp. 1648–1656.
[35] M. Titsias, in *Proc. of the 12th Int. Conf. on Artificial Intelligence and Statistics* (Eds: D. van Dyk, M. Welling), Microtome Publishing, Brookline, MA, USA **2009**, pp. 567–574.
[36] I. M. Sobol, *USSR Comput. Math. Math. Phys.* **1976**, *16*, 236.
[37] A. Saltelli, P. Annoni, I. Azzini, F. Campolongo, M. Ratto, S. Tarantola, *Comput. Phys. Commun.* **2010**, *181*, 259.
[38] V. Deshpande, M. Ashby, N. Fleck, *Acta Mater.* **2001**, *49*, 1035.
[39] T. A. Schaedler, A. J. Jacobsen, A. Torrents, A. E. Sorensen, J. Lian, J. R. Greer, L. Valdevit, W. B. Carter, *Science* **2011**, *334*, 962.
[40] X. Zheng, H. Lee, T. H. Weisgraber, M. Shusteff, J. DeOtte, E. B. Duoss, J. D. Kuntz, M. M. Biener, Q. Ge, J. A. Jackson, S. O. Kucheyev, N. X. Fang, C. M. Spadaccini, *Science* **2014**, *344*, 1373.